


Article

Exploring Copper Resources: A Geophysical and Geological Approach in the South Riogrande Shield, RS, Brazil

Marieli Machado Zago ^{1,2,*} and Maximilian Fries ^{1,2} 

¹ Programa de Pós-Graduação em Geologia, Federal University of Paraná, Curitiba 81531-990, PR, Brazil; maximilianfries@unipampa.edu.br

² Laboratório de Geofísica Aplicada (LGA), Federal University of Pampa, Caçapava do Sul 96570-000, RS, Brazil

* Correspondence: marielizago@gmail.com

Abstract: The search for mineral resources presents an enduring challenge as these demands consistently surge, and the utilization of geophysics is undeniably intertwined with the pursuit of novel prospects. Technological advancements over recent decades have facilitated access to 2D and 3D visualization software, enabling robust data integrations. Consequently, interpreters possess the latitude to harness their ingenuity and technical acumen in conducting multifarious analyses. Mineral exploration in greenfield areas, a particularly challenging endeavor, often commences with regional surveys and circumscribed information about the terrain. Notwithstanding limited preliminary data, the judicious deployment of filtering, modeling, and inversion techniques with geophysical data holds sway in catalyzing discoveries. This study, with its comprehensive amalgamation of diverse copper occurrence indicators and the novel procedural framework it establishes for processing and integrating airborne gamma-ray spectrometry and magnetometry geophysical and geological data, exemplifies the complexity and depth of our field. Elaborate litho-geophysical profiles, linked with data concerning mineral occurrences and geochemistry, pinpoint potential copper deposits in the area. This multidisciplinary approach and inversion mode provide detailed insights into probable mineralized body continuity and regional structural frameworks, offering valuable guidance for future regional mineral exploration efforts.



Academic Editors: Yangkang Chen, Xiaolong Wei and Ziyi Yin

Received: 11 November 2024

Revised: 9 January 2025

Accepted: 13 January 2025

Published: 24 January 2025

Citation: Zago, M.M.; Fries, M. Exploring Copper Resources: A Geophysical and Geological Approach in the South Riogrande Shield, RS, Brazil. *Geosciences* **2025**, *15*, 38. <https://doi.org/10.3390/geosciences15020038>

Copyright: © 2025 by the authors. Licensee MDPI, Basel, Switzerland. This article is an open access article distributed under the terms and conditions of the Creative Commons Attribution (CC BY) license (<https://creativecommons.org/licenses/by/4.0/>).

Keywords: mineral exploration; MVI; data integration techniques; copper occurrences; airborne magnetometry; airborne gamma-ray spectrometry

1. Introduction and Objectives

A new mineral discovery holds immense value, particularly in the context of ever-growing market demands. Metallic minerals, including copper, are highly sought after due to their critical role in advancing modern technologies. Copper in particular is indispensable for sustaining contemporary life, with its applications spanning renewable energy systems, electronics, and infrastructure. However, experts warn of a looming copper scarcity in the coming years, which could lead to significant economic disruptions [1]. This looming crisis underscores the importance of efficient mineral exploration and the development of new mines. Yet, this journey is fraught with challenges, as evidenced by the recent volatility in copper prices, which signals potential constraints on mine development sooner than anticipated. The situation in Chile, one of the world's largest copper suppliers, exemplifies these projections, with major companies facing declining export revenues due to production issues stemming from diminishing ore quality and increased extraction costs.

In light of these challenges, the need for new copper discoveries is more urgent than ever to meet or sustain global demand until alternative energy solutions emerge. However, as [2,3] note, finding significant new deposits has become increasingly difficult. Most large, economically valuable mineral provinces have already been identified, leaving researchers to target deeper and more complex deposits. Modern mineral exploration now relies heavily on advanced equipment, robust software, and data processing techniques capable of creating detailed 3D models. However, success in exploration hinges on integrating these geophysical results with comprehensive geological data, including structural, geochemical, and petrological information.

The state of Rio Grande do Sul (RS) exemplifies the potential for polymetallic mineral exploitation, including copper. Metal exploration in RS began in the early 20th century, gained momentum in the 1960s, and continues today, primarily driven by private sector interest. The state has hosted notable mines such as Minas do Camaquã and Mina Seival, though both are currently inactive. Ref. [4] classified numerous copper occurrences in RS based on their associated lithologies, providing a foundation for subsequent exploration. Building on decades of geological work by the Geological Survey of Brazil (CPRM), which includes mineral resource mapping, lithological studies, geochemical data, and aerogeophysical surveys, this study seeks to refine the understanding of copper occurrences in RS. Despite the regional scale of much of the existing data (1:500,000/1:250,000), the aim is to identify areas with higher potential for localized research.

Geophysical methods such as gamma spectrometry and magnetometry have proven invaluable in copper exploration and characterization. Gamma spectrometry measures the natural radioactivity of rocks and soils, revealing the distribution of elements like potassium, uranium, and thorium, which often indicate hydrothermal alteration associated with copper mineralization [5]. Magnetometry detects variations in the Earth's magnetic field, providing insights into magnetite-rich mineralization and geological structures, such as faults and intrusions, often linked to porphyry copper systems [6]. These methods have been successfully applied in various studies, such as mapping copper-rich lithologies in Zambia's Copperbelt [7] and identifying mineralized zones in the Andes of South America [8].

To advance copper exploration in RS, this study presents a workflow that integrates geological data with processed airborne magnetic and gamma-ray spectrometry geophysical datasets. This integrated approach enables a better understanding of lithological contacts, structural frameworks, and the depth and continuity of magnetic bodies associated with copper occurrences, thereby enhancing the precision and effectiveness of mineral research.

2. Study Area and Geological Settings

The study area is located near the municipalities of Vila Nova do Sul, São Gabriel, and Lavras do Sul in Rio Grande do Sul, Brazil (Figure 1a). Geologically, it is situated in the southern portion of the Mantiqueira Province and is referred to as the South Riograndense Shield (SRGS) (Figure 1b). This region, recognized for its geological characteristics and mineral occurrences, is the result of a process of continental crust generation and deformation, with the most significant contributions occurring during the Transamazonian cycle (2.26–2.00 Ga) and the Brasiliano cycle (900–535 Ma) [9,10].

The SRGS comprises units of the Dom Feliciano Belt established in the Neoproterozoic, represented by the São Gabriel Tijucas and Pelotas Batholith terrains. Additionally, Paleoproterozoic units occur, such as the Taquarembó Terrain and the Tijucas terrain [11] (Figure 1a). Locally, the study area is located within the tectonostratigraphic units of the Taquarembó Terrain and São Gabriel Terrain.

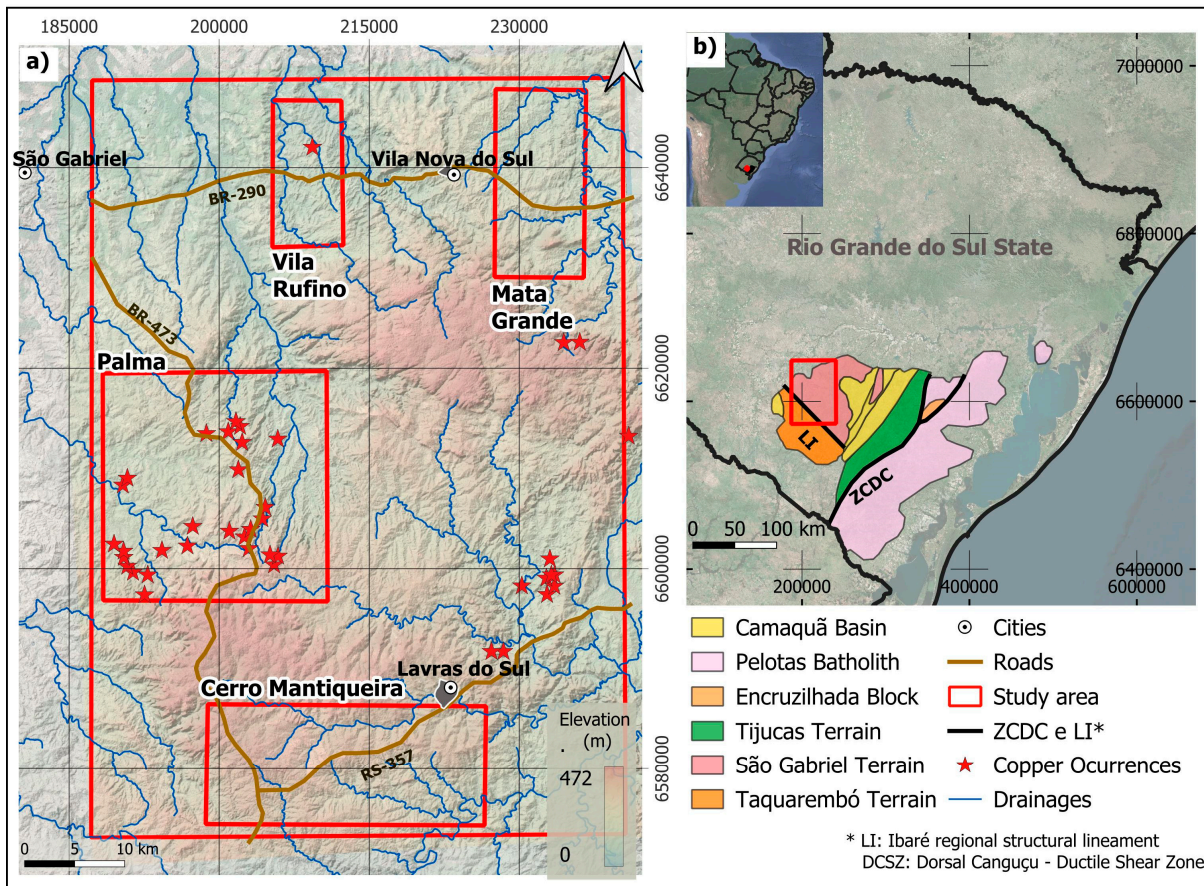


Figure 1. (a) Main access highways and location of copper occurrences in the study area (CPRM, 2021) and (b) map of the state of Rio Grande do Sul, the location of the leading regional geological features and the location of the study area.

The Taquarembó Terrain is represented by the Santa Maria Chico Granulite Complex, predominantly consisting of felsic granulites (trondhjemitic) and mafic rocks, pyroxenites, lenses of harzburgites, sillimanite gneisses, marbles, and calcium-silicate gneisses [11]. Ages of magma accretion for the granulite complex (zircon, SHRIMP) were obtained between 2.5–2.1 Ga, with the collisional event that generated the granulites occurring at 2.02 Ga [12,13].

The São Gabriel Terrain consists of an accretionary prism with petrotectonic associations of passive margin and back-arc environments, ophiolites, volcano-sedimentary magmatic arcs, and plutonic arcs. It is represented by juvenile rocks (meso to Neoproterozoic) including plutonic rocks and low to medium-K calc-alkaline arc rocks (represented by the Cambaí Complex). Zircon ages (TIMS and SHRIMP) range from around 735–680 Ma [13–15]. According to [11], there is also a volcano-sedimentary sequence called the Palma Complex (lower part of the sequence) and the Bossoroca Complex (upper part of the sequence), composed of mafic metavolcanic and associated metasedimentary rocks. The metasedimentary rocks are older than the igneous rocks, but studies suggest they were derived from a juvenile Neoproterozoic source, with little contribution from the older crust. They originated from andesitic sources and basic and felsic arc rock mixtures [11].

The detailed study area (Figure 1a) corresponds to the São Gabriel Terrain, where copper occurrences associated with mafic-ultramafic bodies have been documented. Ref. [4] identified four key areas with mafic-ultramafic bodies for investigation: the Vila Rufino Massif, Mata Grande Massif, Palma Complex, and Cerro Mantiqueira. The Vila Rufino and Mata Grande massifs comprise serpentized dunites and schists, with notable chrysotile

asbestos and minor pyrrhotite occurrences. The Palma Complex exhibits significant disseminated sulfide mineralization and geochemical anomalies, while Cerro Mantiqueira is characterized by magnesian silicate and carbonate sequences containing ultrabasic intrusions.

The Palma Complex is particularly notable for its mineral occurrences and historical geochemical data, with specific sites such as the Passo do Ivo massif, Jazida da Palma, and Cerro Verde offering detailed insights [4,16]. The Passo do Ivo massif hosts disseminated sulfides, including pyrite, chalcopyrite, and pyrrhotite, attributed to metamorphic remobilization and hydrothermal activity. At Jazida da Palma, copper, nickel, and cobalt are associated with ultrabasic masses and contact metasomatism in limestones, producing a mineral paragenesis of pyrite, chalcopyrite, and gold [17]. Cerro Verde features quartz lenses mineralized with magnetite, molybdenite, chalcopyrite, and supergene minerals such as malachite and azurite, linked with quartz and fluorite [16,18]). Ref. [16] also identified additional copper occurrences in the study area, including disseminated and vein-associated chalcopyrite, pyrite, and molybdenite in metamorphic and plutonic rocks, underscoring the region's potential for porphyritic Cu-Mo deposits and related resources.

3. Magnetometry and Gamma-Ray Spectrometry: An Overview of Their Applications in Mineral Exploration

Airborne magnetometry and gamma-ray spectrometry are effective large-scale methods for identifying potential copper mineralization areas. These geophysical techniques detect anomalies associated with copper deposits, aiding exploration efforts. Ref. [19] provided an early overview of geophysical signals characteristic of various deposit types, emphasizing their relevance in mineral exploration. Ref. [20] demonstrated the use of airborne gamma-ray spectrometry data in identifying radiometric anomalies correlated with known copper and iron occurrences. More recently, ref. [21] highlighted the application of filtering and enhancement techniques in processing geophysical data to delineate potential mineral targets.

3.1. Gamma-Ray Spectrometry

The gamma-ray spectrometric method measures the relative abundance or concentration of potassium (K), uranium (eU), and thorium (eTh) in rocks and weathered materials up to 30 cm deep by detecting the gamma radiation emitted from the natural radioactive decay of these elements [22]. According to [22], the average content of radioelements in igneous rocks tends to increase with the silica content of the rock, with felsic rocks having higher concentrations of these radioelements than mafic or ultramafic rocks. The K, eU, and eTh channels generate primary images of these elements for processing gamma-ray spectrometric data. Various products can be derived from the primary images, including channel ratio maps and RGB ternary maps, which are among the most common and efficient techniques. These methods highlight contrasts between the elements, which may be less apparent in the primary maps.

Ref. [23] employed gamma-ray spectrometry to understand pedogenetic processes and the behavior of phosphatic fertilizers. Ref. [24] applied the method to assist in identifying lithological units. Ref. [25] utilized ground gamma-ray spectrometry for geological mapping and distinguishing facies in granitoids.

Gamma-ray spectrometry has also been effectively used to identify copper occurrences by detecting variations in the concentration of radioelements associated with mineralization processes. This method is particularly useful in mapping potassium (K), equivalent uranium (eU), and equivalent thorium (eTh) anomalies, as these elements can indicate hydrothermal alteration zones often linked to copper deposits. High potassium concentrations, for instance, may reflect the potassic alteration characteristic of porphyry copper

systems. Additionally, K, eU, and eTh ratio maps have been employed to delineate alteration halos, highlighting contrasts between mineralized and unmineralized zones. This approach aids in narrowing down prospective areas for exploration and drilling, especially when integrated with geological and geochemical data [26].

In the Bathurst Mining Camp, northeastern New Brunswick, gamma-ray spectrometry has been applied to map various rock types and detect alterations associated with mineralizing hydrothermal systems, aiding in the exploration of massive sulfide deposits [27]. In the Gebel Monqul area of Egypt, the coherence between copper mineralization and uranium enrichment has demonstrated the effectiveness of gamma-ray spectrometry in copper exploration [28]. More recently, ref. [29] described the effective use of gamma-ray spectrometry as an exploration tool in conjunction with geochemical analyses for identifying and quantifying potential targets.

By integrating gamma-ray spectrometry with other geophysical and geochemical methods, exploration efforts can more effectively target copper mineralization.

3.2. Magnetometry

The magnetometry method is essential for understanding the continuity of bodies with magnetic signatures, such as mafic and ultramafic rocks, as well as bodies with sulfidation. It also plays a crucial role in understanding the structural framework, helping to map and identify key geological features. Magnetometry is particularly effective in identifying and mapping ore bodies associated with magnetic minerals, such as magnetite and pyrrhotite, and in delineating structures like faults, folds, and intrusive bodies, which are often related to mineralization [30]. Integrating magnetometric data with other geophysical methods, such as gamma-ray spectrometry and electromagnetic surveys, enhances the accuracy of geological models, reduces exploration risks, and improves the identification of potential mineral targets. The ability to conduct surveys over large areas quickly and cost-effectively makes magnetometry indispensable in greenfield and brownfield exploration settings [30].

Magnetometry has proven to be a powerful tool in copper exploration, especially in complex geological settings. Airborne methods such as electromagnetic (AEM), magnetic surveys, and Induced Polarization (IP) are employed to identify porphyry copper deposits. These techniques help detect subtle electromagnetic signatures of disseminated sulfides and structural features associated with mineralization. For instance, the Mt. Milligan Au-Cu deposit in Canada demonstrated how geophysical tools can map concealed ore bodies, enhancing the ability to target economically viable mineral deposits through advanced data processing and integrated exploration strategies [31].

Additionally, these methods aid in delineating geological structures like faults, folds, and intrusive contacts, which are key features controlling copper distribution. Refs. [32,33] showcased the effectiveness of aeromagnetic data in structural and geological mapping, identifying new areas of potential mineralization for exploration. Integrating geophysical data, such as airborne magnetic surveys, electromagnetic methods (e.g., ZTEM), and helicopter TDEM, is essential for identifying porphyry and SEDEX copper deposits. Discrete magnetic anomalies often correlate with hydrothermal magnetite in potassic alteration zones of Cu-Au porphyry deposits.

Gravity and magnetic surveys play a crucial role in IOCG systems, as evidenced by the discovery of the Olympic Dam deposit through coincident anomalies. Structural complexity analysis enhances target selection by highlighting structurally controlled mineralizations. These geophysical methods and AIP effects help delineate hydrothermal alteration zones critical for copper exploration [34].

Furthermore, magnetometric surveys have been successfully applied in various regions, including significant iron deposits in Victoria. These deposits, concentrated in

the Buchan Rift, are primarily replacement deposits in Silurian sediments and the basal Snowy River Volcanics. Initially explored for iron ore and later for copper and gold, they exhibit intense magnetic responses. The Five Mile deposit, identified from 1950s surveys, revealed about 6 Mt of magnetite-haematite mineralization. The Three Mile prospect, discovered in 1983, showed promising copper intersections, including 5.2 m at 4.8% copper. Induced polarization surveys helped define mineralized areas, although pyrite responses can overshadow subtle chalcopyrite signals. The complex geology suggests these may be sulfur-poor massive sulfide deposits, offering further exploration opportunities [35].

4. Material and Methods

For the development of this study, four main stages were defined and are detailed in Figure 2.

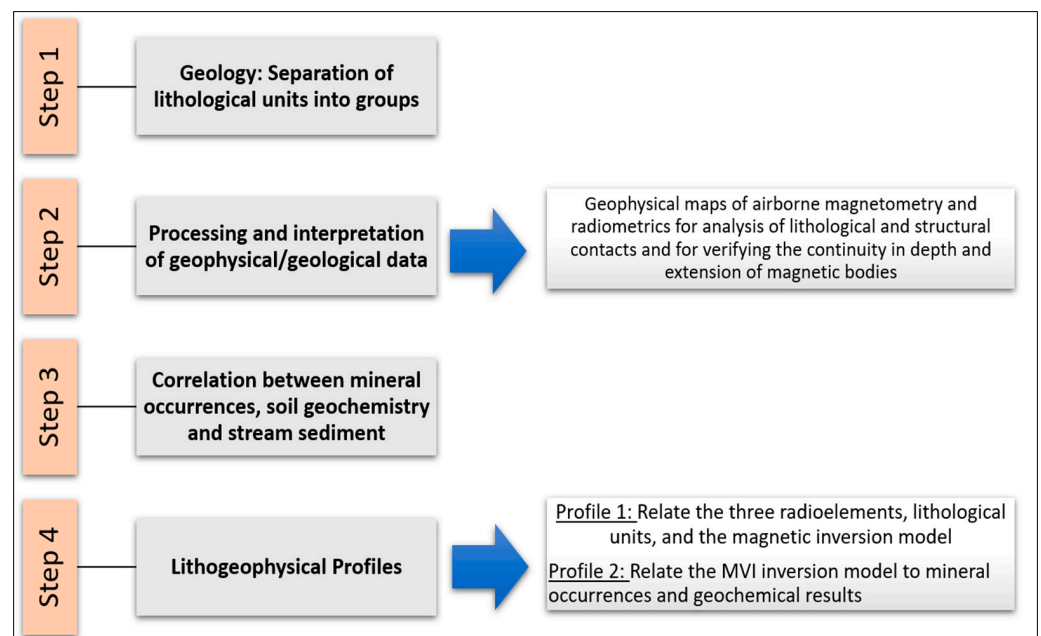


Figure 2. Flowchart of activities divided into four stages.

The study began by grouping lithological units into five major representative rock categories based on similar petrographic characteristics and formation ages (Step 1). This initial step was crucial for organizing the data and creating a framework for interpreting the geological context. By compartmentalizing the lithological units, researchers could better align their geological observations with geophysical signatures, facilitating a clearer understanding of the region's geological history and processes.

Following this, geophysical surveys, including airborne gamma-ray spectrometry and magnetometry, were conducted alongside structural analysis (Step 2). These surveys generated detailed geophysical maps that were instrumental in identifying lithological and structural contacts. Furthermore, the data provided insights into magnetic bodies' continuity in depth and lateral extension. This analysis was key to unraveling the subsurface structure and identifying areas of potential geological interest.

To deepen the understanding of the region, correlations were established between mineral occurrences, soil geochemistry, and stream sediment data (Step 3). This integration of datasets allowed researchers to link surface geochemical patterns with subsurface geological features. Such correlations are essential for identifying mineralization zones and understanding their spatial relationships within the geological framework.

Finally, two lithogeophysical profiles were developed to consolidate the findings (Step 4). The first profile integrated data from three radioelements, lithological units, and a magnetic inversion model, offering a comprehensive representation of subsurface characteristics. The second profile focused on connecting the Magnetic Vector Inversion (MVI) model with mineral occurrences and geochemical results, further refining the interpretation of potential exploration targets. These profiles provided a robust basis for geological analysis and exploration strategies.

The materials used for this study were derived from geophysical, geochemical, and lithological investigations conducted by the Brazilian Geological Service (CPRM) and are freely accessible.

For the processing and interpretation of aeromagnetic and gamma-ray spectrometry data, the database from the Rio Grande do Sul Shield Project (scale 1:250,000) by the Geological Survey of Brazil—CPRM was utilized. The acquisition parameters for the aerogeophysical survey included flight lines oriented in an N–S direction, with a 500-m spacing and an average flight altitude of 100 m [36].

The geochemical data comprised 48 soil sampling points and 47 stream sediment samples, collected as part of the Geochemical Survey Project of Rio Grande do Sul conducted in 1976 and updated in 2021 by CPRM.

The raw geophysical data was processed by [36], which includes the removal of the IGRF and corrections in the gamma-ray spectrometric data. The geophysical maps were generated using the Oasis Montaj software (version 2024.1). The VOXI extension was used to create 3D models of magnetic data employing the vectorial magnetization model type Magnetization Vector Inversion (MVI).

For the MVI inversion, cell sizes in X, Y, and Z of 240, 245, and 35, respectively, were considered. The input data considered was the magnetic field reduced to the IGRF; no constraints or weights were added for any type of parameter to avoid bias in the final result. Likewise, magnetization values of groups of rocks were not considered since no previous petrophysical studies were carried out. Additional processing included creating Analytic Signal (AS) and first vertical derivative (1DVz) filters, along with a ternary RGB map derived from gamma-ray spectrometric data. Structural lineaments were manually interpreted from the First Vertical Derivative maps, resulting in a rosette diagram illustrating the lineament trends. QGIS software (version 3.34.9-Prizren) was employed to integrate and interpret geophysical and geological data.

Geophysical Data Processing for Copper Occurrence: Theoretical Insights, Evolution, and Effectiveness

Filters such as the analytical signal and the first vertical derivative are essential for enhancing magnetometric data in copper occurrence research. The analytical signal, introduced by [37], combines the gradients of the magnetic field in all three spatial directions, creating a signal independent of the magnetization direction. This property is particularly valuable for identifying subsurface structures and delineating magnetic body edges. Later works, such as [38,39], expanded on its application, demonstrating its utility for semi-automatically interpreting 2D sources, especially in low magnetic latitudes or areas with complex remanent magnetization. Meanwhile, the first vertical derivative enhances high-frequency components of the data, improving the resolution of shallow magnetic sources [40]. Together, these filters enable geoscientists to analyze geological structures associated with copper mineralization more effectively, particularly when integrated with lithological and geochemical datasets [41].

The processing of magnetometric data requires careful consideration of spatial and temporal variations, anomaly separation, and interpretation techniques to ensure high-resolution results. Early researchers such as [42,43] developed simple methods for anomaly

separation, including graphical smoothing and analytical grid systems. Refs. [44,45] later introduced processing schemes in the frequency domain to refine residual separation techniques. Ref. [46] emphasized the importance of isolating and enhancing anomalies while addressing directional attributes, gradients, and correlations with geological or geophysical variations. These advancements have laid the foundation for modern data interpretation in magnetometry.

The analytical signal (AS), as described by [37,47,48], has been widely used to locate and determine the depth of magnetic anomaly sources. Applications include interpreting dyke bodies [49] and addressing non-directed remanent magnetization in areas with complex geophysical characteristics [38]. Hilbert transform pairs, discussed by [39], further refined the application of AS in large datasets, making it an indispensable tool in mineral exploration.

Magnetic vector inversion (MVI) techniques have evolved significantly over recent decades. Ref. [50] discuss significant advancements in geophysical data inversion, which are essential for mineral exploration. The inversion methods are categorized into three types: Type I (discrete body), Type II (pure property), and Type III (lithologic). Equation (1) represents the misfit function in the inversion process, focusing on minimizing the difference between observed and predicted data.

$$\Phi_d = \sum_{i=1}^N \left(\frac{d_i^{obs} - d_i^{pred}}{\sigma_i} \right)^2 \quad (1)$$

where d_i^{pred} is predicted data, d_i^{obs} is predicted observations, and N is the number of data. Equation (2) describes the model's objective function, incorporating smoothness and proximity to a reference model.

$$\begin{aligned} \Phi_m(m) = & \alpha_s \int_{\Omega} W_s (m - m_{ref})^2 dv + \alpha_x \int_{\Omega} W_x \left[\frac{d(m - m_{ref})}{dx} \right]^2 dv + \\ & \alpha_y \int_{\Omega} W_y \left[\frac{d(m - m_{ref})}{dy} \right]^2 dv + \alpha_z \int_{\Omega} W_z \left[\frac{d(m - m_{ref})}{dz} \right]^2 dv \end{aligned} \quad (2)$$

where m_{ref} is a reference model, the α coefficients control the relative importance of smoothness in the various directions compared with closeness to a background, and the W 's are weighting functions.

The use of depth weighting (Equation (3)) is mentioned as a technique to overcome the inherent limitations of potential field data, which lack depth resolution.

$$w(z) = 1/(z + z_0)^{v/2} \quad (3)$$

where z_0 is a constant that depends upon flight height and cell size, and $n = 3$ for magnetic data. Since the fields decay as $1/r^2$, the exponent would be $n = 2$ for gravity data.

According to [50], integrating geological models and continuously improving computational techniques is paramount. They highlighted potential methods as economical, high-resolution approaches for investigating subsurface structures.

Issues related to magnetic susceptibility inversions, including the influence of remanent magnetization, were discussed by [51,52], who proposed solutions for improving inversion accuracy.

Ref. [51] address challenges in interpreting magnetic data due to unknown remanent magnetization directions. The authors propose an inversion algorithm that minimizes dependence on magnetization direction by utilizing total gradient data. Equation (4)

defines the total gradient g as the square root of the sum of squares of the partial derivatives of the anomalous magnetic field.

$$g = \|\nabla B\| = \sqrt{(\partial B/\partial x)^2 + (\partial B/\partial y)^2 + (\partial B/\partial z)^2} \quad (4)$$

where B is a given component of the anomalous field, such as the total field anomaly or the vertical anomaly.

The inversion problem is formulated using Tikhonov regularization (Equation (5)), which combines a data misfit term Φ_d and a model objective function Φ_m , controlled by a regularization parameter β .

$$\Phi = \Phi_d + \beta\Phi_m \quad (5)$$

The methodology incorporates a positivity constraint through a logarithmic barrier method (Equation (6)), ensuring non-negative magnetization values.

$$\Phi = \Phi_d + \beta\Phi_m - 2\lambda \sum_j \ln \kappa_j \quad (6)$$

The algorithm employs a Gauss–Newton approach for iterative minimization (Equation (7)), efficiently calculating the sensitivity matrix necessary for updating the model parameters.

$$(J^T W_d^T W_d J + \beta W_z^T W_z + \lambda X^{-2}) \Delta \vec{\kappa} = -J^T W_d^T W_d \delta \vec{d}^n - \beta W_m^T W_m \delta \vec{\kappa}^n - \lambda X^{-1} \vec{e} \quad (7)$$

This approach allows for effective 3D inversion of magnetic data, offering practical applications in fields like petroleum exploration, kimberlite imaging, and crustal studies.

More recently, ref. [53] introduced Magnetization Vector Inversion (MVI), which incorporates induced and remanent magnetization without prior knowledge of remanent magnetization properties. This innovation has been tested in mineral exploration and demonstrated greater accuracy in interpreting magnetic field data.

This technique improves the interpretation of magnetic field data by incorporating both remanent and induced magnetization without prior knowledge of the remanent magnetization's direction or strength. The study highlights that traditional voxel-based inversion methods often assume only induced magnetization, leading to potentially misleading interpretations due to the significant presence of remanent magnetization in crustal rocks and mineralized zones.

Key equations include the magnetic field calculation from a volume magnetization (Equation (8)) and the objective function for inversion with Tikhonov regularization (Equation (5)).

$$B(r) = \mu_0 \int_V \frac{M(r') (r - r')}{|r - r'|^3} dV' \quad (8)$$

Through examples with synthetic and real data, including a case study of the Cu–Au Osborne deposit, the authors demonstrate the efficacy of MVI. The results show that incorporating remanent magnetization significantly improves the accuracy of magnetic data interpretation. The study concludes that ignoring remanent magnetization can lead to misleading interpretations, highlighting the need for comprehensive approaches like MVI in magnetic field data inversion.

5. Results and Discussions

The results and discussions were divided into the following topics: (i) Separation of lithological units into groups; (ii) Processing of aeromagnetometric and aerogamaespectrometric data; (iii) Integration of geophysical data and information on mineral occurrences, soil geochemistry, and stream sediment; and (iv) Generation of lithogeophysical profiles.

5.1. Separation of Lithological Units into Groups

The lithological units were compartmentalized into five major representative rock groups with similar petrographic characteristics and formation ages. This step aims to better interpret the geological context with the geophysical signatures (Figure 3).



Figure 3. (a) Map of lithological units, (b) map of group separation. Adapted from [16].

The five groups were compartmentalized with similar lithologies described by [16] (Figure 3):

Ultramafic Rocks: rocks that have undergone intense regional metamorphism, such as metamafites, metagabbros, serpentinites, and magnesian schists with ages of ~850–630 Ma. The units known as Bossoroca, Arroio Lageadinho, Arroio Cambaizinho, Passo do Ivo, and Palma have been integrated with rocks belonging to the Cerro Mantiqueiras Formation, composed of metamafites, serpentinites, metagabbros, and magnesian schists, with ages also ranging from ~850–630 Ma.

Mafic/Intermediate Rocks: represented by gabbros, tonalites, trondhjemites, diorites, amphibolites, and granodiorites with ages ranging from ~1000–730 Ma. The units that compose this large group are the Vila Nova do Sul Suite, Lagoa da Meia Lua Suite, and Passinho Suite.

Plutonic Igneous Rocks: represented by granitoids such as monzogranites, granodiorites, and syenogranites with ages of ~650–540 Ma, referred to as the Ramada Granite, Camaquã Pelado Syenogranite, São Manoel Granite, Santa Rita Monzogranite, Jaguarari Granite, and Lavras do Sul Intrusive Suite.

Volcaniclastic Rocks: This group is composed of volcaniclastic igneous rocks, which have eventually undergone regional metamorphism. Representative units include the Ibiajutura Formation, consisting of metasandstones, mica schist, phyllite, and slate, with ages ranging from 1000 to 635 Ma. Also, the Acampamento Velho Formation, mainly composed of rhyolites, tuffs, pyroclastic breccias, and ignimbrites with an age of ~650–540 Ma, the Arroio dos Nobres Formation composed of conglomerates, siltstones, and sandstones with an age of ~650–540 Ma, the Pontas do Salso Formation with metatuffs and epiclastic

metasedimentary rocks with an age of ~850–630 Ma, and the Hilário Formation mainly composed of andesites with an age of ~650–540 Ma.

Sedimentary Rocks: Comprised of sandstone, siltstone, and conglomerate with ages ranging from ~318–270 Ma in rocks belonging to the Guatá Group and from ~650–540 Ma in rocks of the Maricá Group.

5.2. Airborne Gamma-Ray Spectrometry, Airborne Magnetometry, and Structural Analysis

Maps of the three radioelement channels K, eTh, and eU and an RGB Ternary map were generated from the gamma-ray spectrometry data made available by [36] (Figure 4a–c). For the interpretation of the maps, the lithological group map will be used (Figure 4d). The study area presents strongly delineated lithological units in the RGB Ternary map (Figure 4e). The granitoids of the plutonic igneous rock group are delineated by the high counts of the elements (whitish colors) and higher counts of the potassium and thorium elements. It is observed that the ternary map delimits the boundaries of the metamorphosed mafic/ultramafic rocks, which have low total element counts (dark colors).

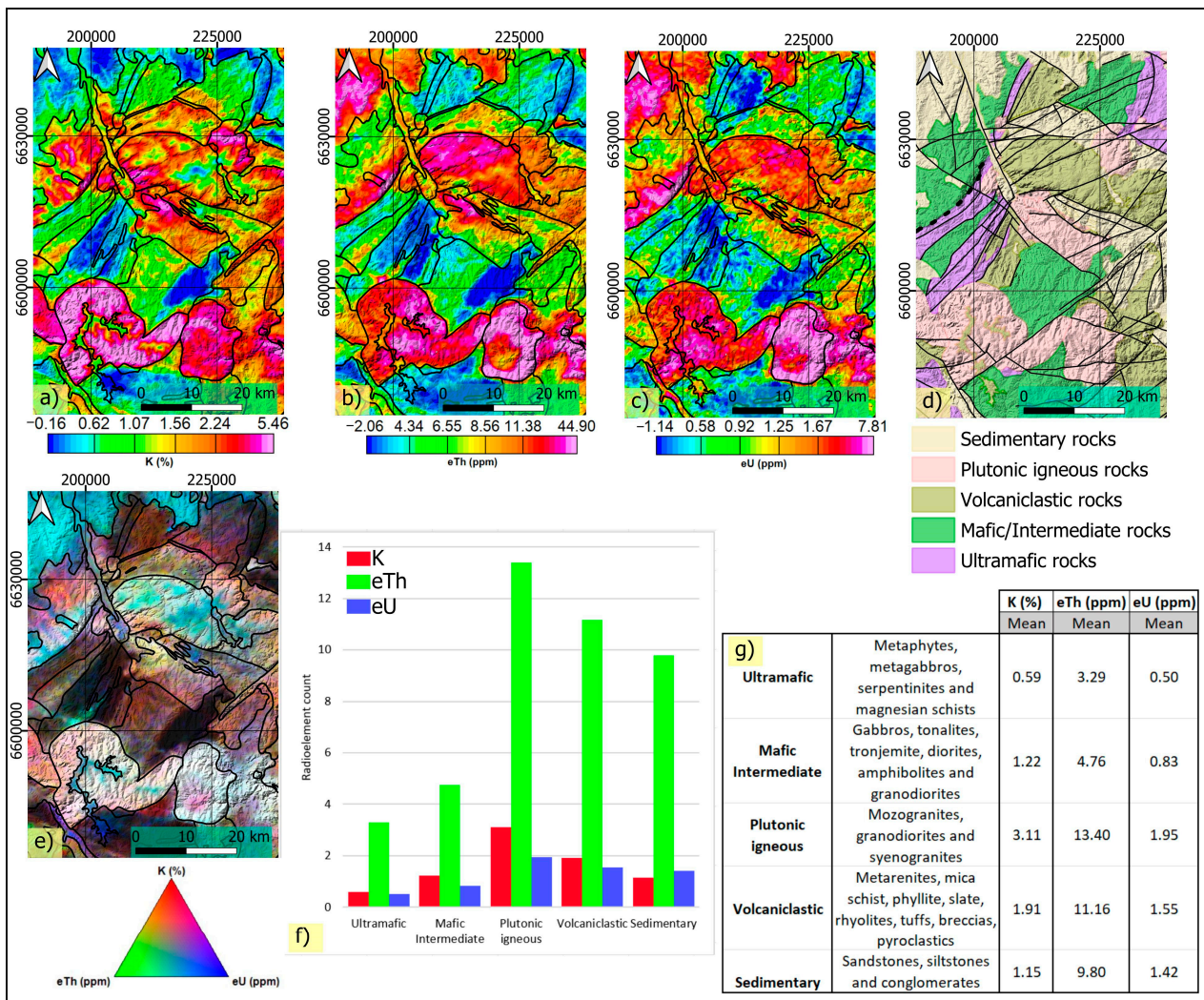


Figure 4. (a) Potassium Channels, (b) Uranium, (c) Thorium, (d) Lithological Group Map, (e) RGB Ternary Map, and (f) Histograms showing the variation of the mean values of eTh, eU, and K concerning the rock groups in the area of interest (the colors represent: K, red; eTh, green; eU, blue), and (g) the table with the average radioelement values for each rock group.

The Mafic/Intermediate rock group shows K, eU, and eTh variations. These variations can be observed in Figure 4a–c. Rocks with higher potassium element counts are related to plutonic igneous rocks (granodiorites and monzogranites) (Figure 4a).

The sedimentary rock group shows a more significant variation in radioelements, generally exhibiting higher values, although some have a higher potassium percentage. These are associated with siltstones, conglomerates, and sand. Sedimentary rocks in contact with mafic and ultramafic units have a higher concentration of mafic minerals and low silica content, facilitating a signature with low counts of K, eU, and eTh.

The histograms of radioelement countings and the table with the average radioelement values for each lithotype show significant dispersion and variability (Figure 4f,g). This occurs due to various factors, including flight altitude, thickness of the soil cover, presence of dense vegetation, and variation in mineralogical composition for each lithotype. Despite the considerable variability, patterns can be observed. The group of plutonic igneous rocks has the highest element count in all channels, confirming that the higher the silica content in the rock composition, the higher the radioelement count. In contrast, ultramafic rock groups behave oppositely, showing low radioelement counts.

From the aerial magnetometry database, the Total Magnetic Intensity (TMI) map and Analytic Signal (AS) map were generated (Figure 5a,b). The results show striking contrasts in the magnetic signature in the TMI map with dipolar regions, and circular structures corresponding to the Ramada Granite, Lavras do Sul Granite, and Jaguari Granite are observed. The AS map highlights mafic and ultramafic lithological units and exhibits intense magnetic signatures. Plutonic igneous and sedimentary rock bodies show a weak magnetic signature.

A First Vertical Derivative filter was applied (Figure 5d) to highlight the region's structural framework (Figure 5e). Ultramafic bodies, mafic/intermediate igneous rocks, and volcanoclastic rocks show structural solid control (Figure 5c). The results of structural interpretations and comparisons with measurements made by [16] reveal a NE–SW structural trend (Figure 5g). Plutonic igneous lithological units and sedimentary rocks do not show intense structural control (regions identified in Figure 5e in pink color).

Since ultramafic rocks exhibit magnetic contrast compared to other lithologies and have the most significant potential to host mineralization, the Magnetization Vector Inversion (MVI) technique was applied to understand the continuity of subsurface bodies laterally and in-depth and the inclination of lithological bodies (strike and dip) (Figure 5f).

Through the analysis of the MVI inversion results of the aeromagnetic data along with the structural context described by [16], it is observed that ultramafic lithological units have a preferential direction of N45° E and a dip of 50°, which is also observed in depth (Figure 5f).

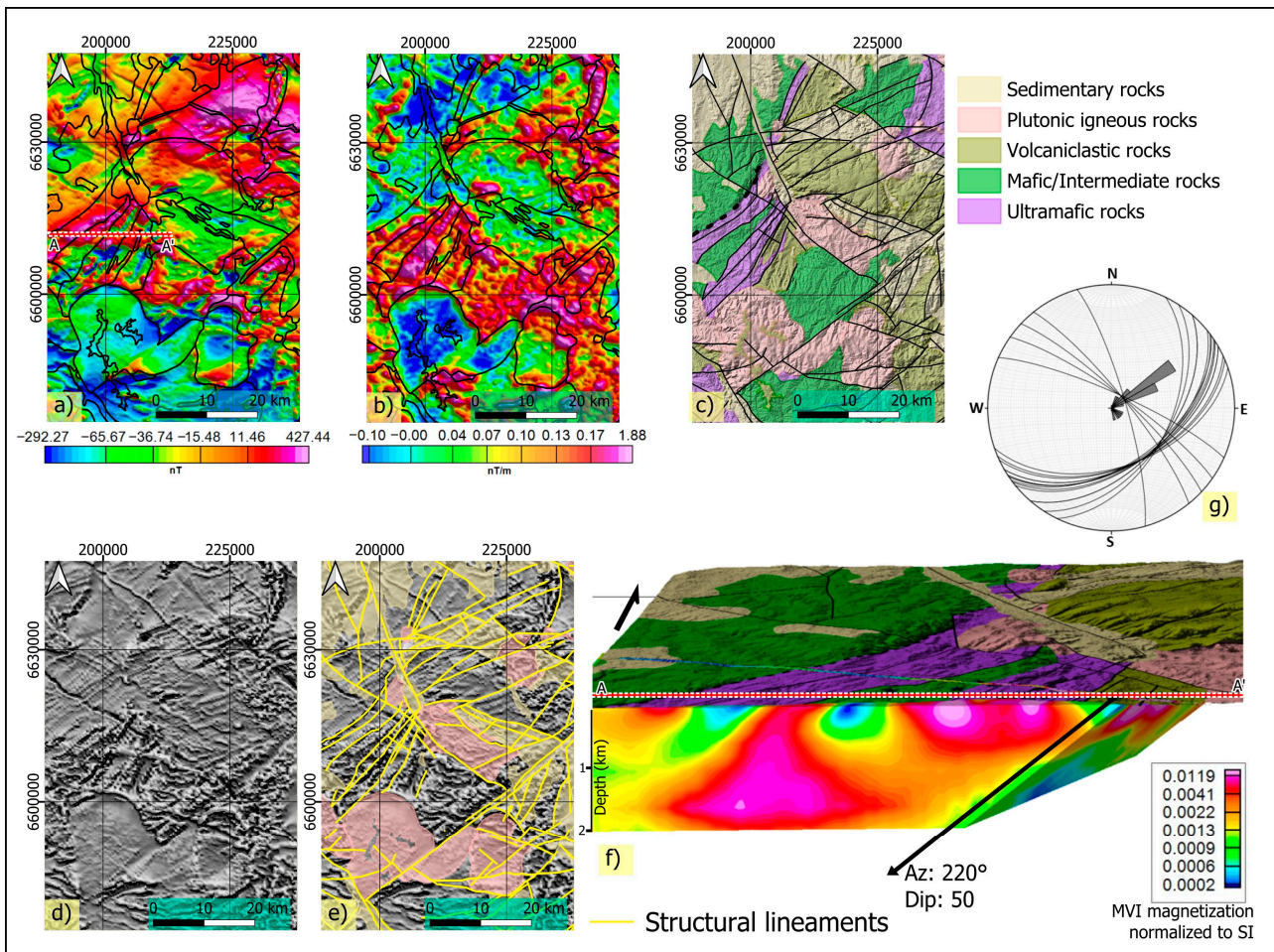


Figure 5. (a) Total Magnetic Anomaly Field Map and indication of the location of the cross-section A–A', (b) the Analytic Signal Map, (c) Lithological Group Map with structural context (CPRM, 2021), (d) First Vertical Derivative Map (1DVz), (e) 1DVz Map highlighting structural lineaments and plutonic rocks, (f) Cross Section A–A' of the MVI Inversion Model, and (g) Rosette Diagram.

5.3. Mineral Occurrences, Soil Geochemistry, and Stream Sediment Analysis

Ribeiro (1978) [4] identified potential areas containing mafic-ultramafic bodies, among which four areas were selected for detailed geological study: the Vila Rufino Massif, Mata Grande Massif, Palma Complex, and Cerro Mantiqueira (Figure 6a).

The Vila Rufino Massif consists of small bodies of serpentinized dunites in contact with magnesian schists (serpentine-chlorite-talc schists). These are considered products of retro-metamorphism acting on the ultrabasic and basic rocks of the Cerro Mantiqueira Formation. A small occurrence of chrysotile asbestos is known in the southern part of this massif. The entire massif (dunites and schists) measures 12×5 km and is in tectonic contact with rocks of the Cambaí subgroup (gneisses and granites) through two parallel faults oriented $N20^\circ E$.

The Mata Grande Massif consists of an elongated area measuring 18×2.5 km with significant occurrences of serpentinized dunite bodies embedded in schistose rocks, trending $N20^\circ E$, and is responsible for the contact between the Cerro da Mantiqueira Formation and the chlorite schists of the Vacacaí subgroup (to the east) and the gneisses of the Cambaí subgroup (to the west). Occurrences of chrysotile asbestos are recorded at the southern end of the body, and there is knowledge of pyrrhotite, rare and finely disseminated in serpentinites, and talc-chlorite-tremolite schists [54].

The Palma complex consists of three main occurrences: Passo do Ivo, Jazida da Palma, and Cerro Verde, containing records of disseminated sulfidation and geochemical results from stream sediment and soil samples.

The Cerro Mantiqueira occurrence consists of an elongated body measuring 5.6×0.4 km, composed of a silicate magnesian sequence (chlorites, talc-chlorite schists, hornblende-tremolite, actinolite schists, tremolitites) and, concordant with it, a carbonate magnesian sequence (limestones with giobertite, dolomites with olivine, and limestones with ankerite). Within these sequences, oriented N70° E, ultrabasic cores appear (lherzolites, harzburgites, dunites, and serpentinites). Homogeneous basic and acid migmatites of the Cambaí subgroup enclose all these lithological sequences.

To understand the continuity of ultramafic bodies and improve the resolution of inversions, inversion models (MVI) were generated for each area related to the ultramafic bodies described by [4] (Figure 6b). It can be observed that all of them correlate satisfactorily with lithological and structural information. The bodies that stood out due to their excellent continuity in depth and extent are located in the region known as Palma. Various mineral occurrence records and geochemical studies are also found in this locality. Based on these premises, the Palma region will be detailed in terms of geophysics and detailed information about the mineral paragenesis present in registered occurrences in the region.

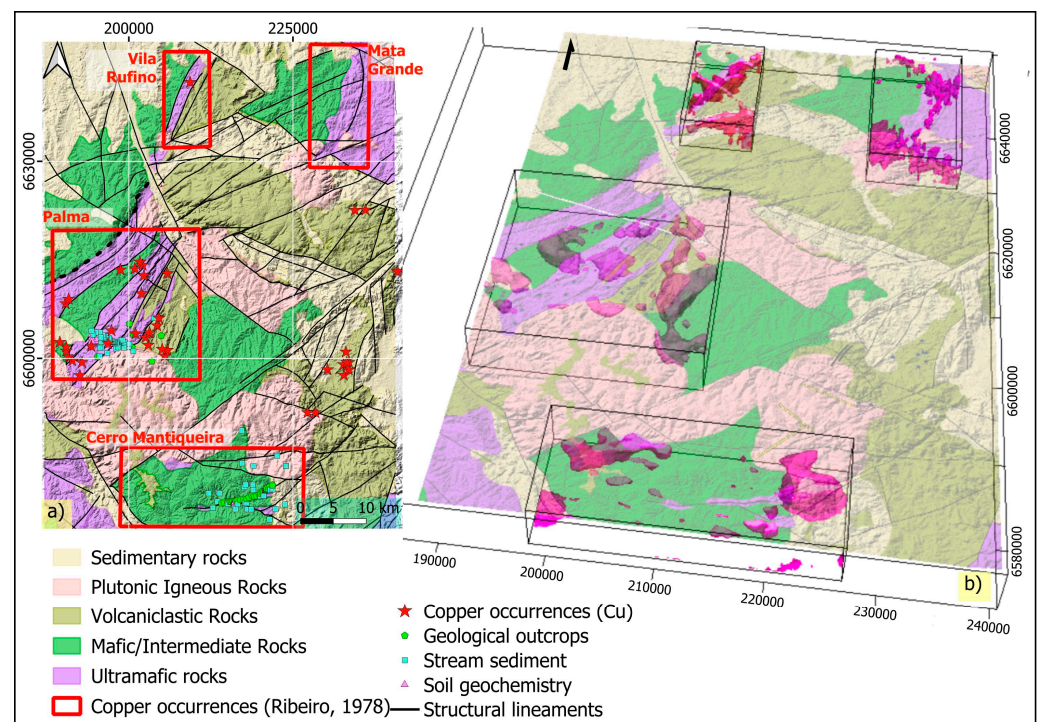


Figure 6. (a) Areas with mineral occurrences hosted in ultramafic bodies. (b) MVI inversion models for the four areas.

5.4. Palma Region—Occurrences and Geochemistry Information

The information that will be described below is very important for understanding in more detail the cupriferous occurrences in the Palma Region. As previously described, minerals have different magnetic signatures. To understand the contrasts in physical properties, it is important to describe the details of the lithotypes. In addition, historical measurements of stream and rock sediment were detailed, which will be used as integration and validation tools for geophysical data.

Figure 7 details and presents occurrences and geochemical information for this specific area. According to [4], the Passo do Ivo massif contains disseminated sulfides, such as

pyrite, and, in smaller proportions, chalcopyrite and pyrrhotite. Ref. [16] states that the occurrences are related to metamorphic remobilization and hydrothermalism.

Jazida da Palma occurs in the Palma Complex and has a gabbro apophysis introduced into marbled limestones. According to [17], in Jazida da Palma, there is an intrusion of an epidotized porphyritic gabbro dyke, with a thickness ranging from 10 to 15 m, which emits numerous apophyses. These apophyses intrude along the finishing planes of the limestones and are folded together with them. The lithology of these apophyses is currently formed by a schist to serpentine, chlorite, and biotite and can be classified as a metabasite.

The intrusion developed contact metamorphism, reaching around 2 m in thickness. In the surrounding limestones, there is a mineral paragenesis based on diopside, tremolite, grossular, sphene, and epidote, in addition to sulfide metallic minerals. These are found in basic rocks and limestones but are always confined to the contact zone. Pyrite is the most abundant sulfide, accompanied by chalcopyrite, pyrrhotite-pentlandite, and gold [17].

Studies conducted by the Departamento Nacional de Pesquisa Mineral (DNPM) indicated a mineral paragenesis concerning sulfides: pyrite, chalcopyrite, arsenopyrite, sphalerite, pyrrhotite, and magnetite. Pyrite is the most abundant sulfide, followed by chalcopyrite; the others are rare.

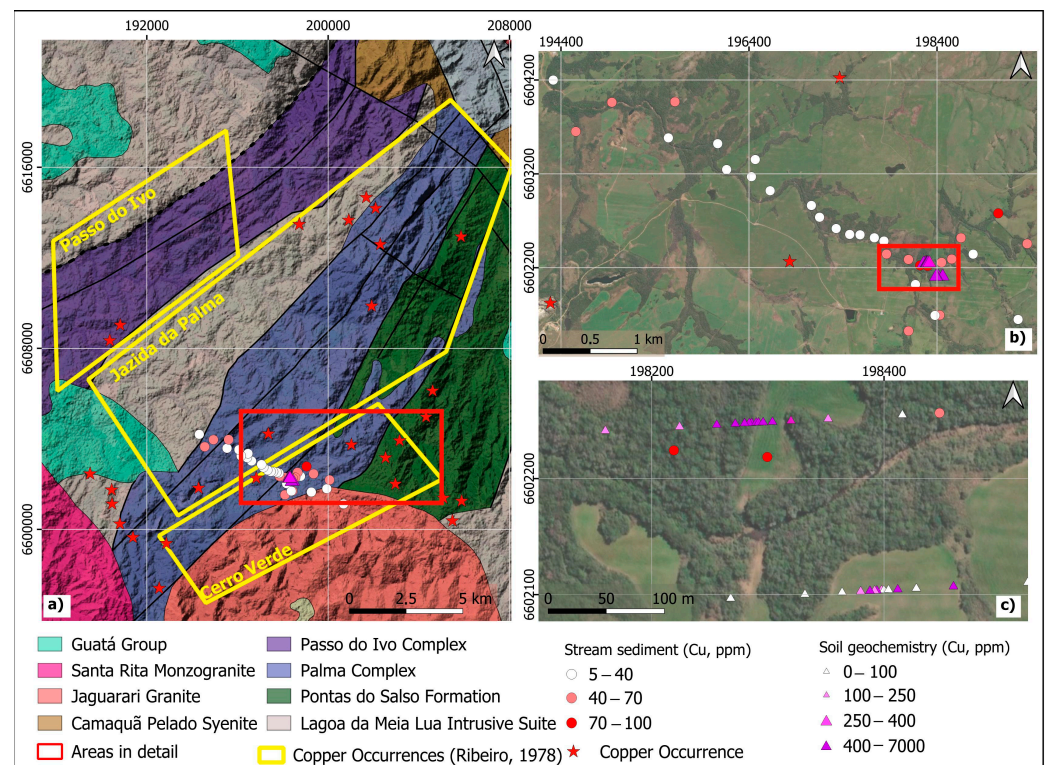


Figure 7. (a) Lithological map with records of Cu occurrences, stream sediment, and soil geochemistry, (b) detailed location of stream sediment samples, and (c) detailed profiles of the two soil sampling points; adapted from [4,16].

Ref. [4] argues that Jazida da Palma has two favorable conditions for copper, which are possibly genetically related:

- (1) Copper, with nickel and cobalt, linked to ultrabasic masses.
- (2) Copper in deposits originating from the contact metasomatism of these bodies on the limestones of the sedimentary sequence.

The occurrence known as Cerro Verde is located in the western region of the Jaguarari Granite and in contact with the host rock, mainly the Palma Complex [4]. Quartz lenses

with a direction of N45° E were described in this occurrence and were associated with migmatites. The mineralization is found in scattered pockets in the quartz lenses [18]. The ore mineralogy consists of magnetite, molybdenite, chalcopyrite, bornite, pyrite, and gold (primary ore), and chalcocite, covellite, cuprite, malachite, and azurite (supergene) have also been identified. All these minerals are associated with quartz, fluorite, calcite, and epidote.

Ref. [16] indicates 28 occurrences of copper in the area of interest, which measures 22 × 22 km. In the Passo do Ivo metamorphic complex, two occurrences are described. Most occurrences are near the contact between the Jaguari Granite, the Palma Complex, and the Pontas do Salso Formation. Disseminated concentrations of minerals such as chalcopyrite, pyrite, pyrrhotite, and hematite associated with veins at the contact of the Granite with the Pontas do Salso Formation have been described. At the contact of the granite with the Palma Complex, there are records of copper mining activities as the primary substance and gold and molybdenum as secondary substances. Ref. [16] shows a porphyry Cu-Mo deposit with disseminated mineralizations in metamorphic rock and plutonic igneous rocks such as Monzogranite. The occurrence has mineralogical associations with gold, bornite, chalcopyrite, pyrite, molybdenite, magnetite, fluorite, calcite, and epidote. Other unexploited occurrences have been described in the region, some with mineralogical associations with chalcopyrite, pyrrhotite, and pyrite, possibly associated with faulting in the N45° E direction.

For the study area, 48 soil sampling points and 47 stream sediment samples were used, and 31 elements were analyzed by emission optical spectroscopy. This study is part of the Projeto Levantamento Geoquímico do Rio Grande do Sul (Geochemical Survey Project of Rio Grande do Sul) carried out in 1976 and revised in 2021 by CPRM.

The soil sampling was acquired in the residual soil, considering only horizon A. The collection is mainly concentrated in two profiles with a length of 260 m and a spacing between profiles of 150 m. The results show a variation of Cu from 0 to 7000 ppm, with continuous measurements within a range of 400 to 7000 ppm. Other collections were acquired randomly throughout the area and did not present significant results, ranging from 5 to 40 ppm (Figure 7c).

The stream sediment was collected in a drainage with an NW–SE direction, and the Cu results showed a variation from 5 to 100 ppm. Higher concentrations of Cu occur near the soil sampling profiles, in areas corresponding to the contact between the Jaguari Granite and the Palma Complex (Figure 7b).

5.5. Data Integration Litho-Geophysical Profiles Analysis

Two profiles were generated based on the previously presented information (Figure 8). Profile A–A'' is 22 km long and cuts through all lithological groups, while profile B–B'' is 2.5 km long and focuses on the zone where geochemical information is available (Figure 8).

For the analysis of Profile A–A'' (Figure 9), the following elements were used:

- (i) MVI inversion model that presents the signal intensity variation based on the contrast of MVI magnetization normalized to magnetic susceptibility (SI), which means that the generated anomalies can be directly related to the magnetic susceptibility of materials;
- (ii) A graph with the three radioelements (K, eTh, and eU) and the terrain elevation showing signal intensity, varying from low to high intensity.

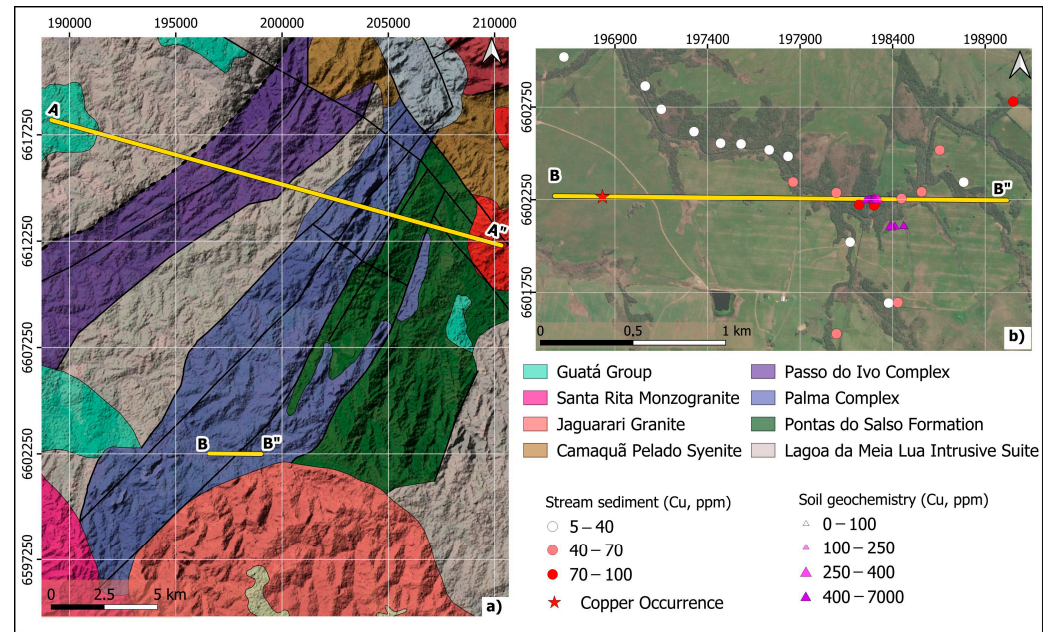


Figure 8. (a) Location map of litho-geophysical profiles and (b) detail of the location of Profile B–B'' with information on stream sediment and soil samples.

In the first 3 km of the profile (Figure 9c), it is observed that the radioelements signature is intermediate, and the MVI inversion presents weak anomalies, which is typical of sedimentary rocks such as sandstones and siltstones. From 3 to 7 km of extension, intermediate mafic rocks represented by tonalite, diorite, and granodiorite of the Lagoa da Meia Lua Formation show a significant increase in radioelements, marking the lithological change, and the MVI inversion has an intermediate signature. The meta ultramafic rocks of the Passo do Ivo Formation, represented by magnesian schists and amphibolites, are strongly delineated in the magnetic signature of the MVI model, with a thickness of approximately 3.5 km, showing a low count of radioelements demarcating the lithological change.

Two circular and continuous low anomalies are observed in the direction of the mapped structures as a sinistral shear zone and a sinistral strike-slip fault or shear zone. The magnetometry method and detected anomalies are characterized by identifying structures and mainly demarcating those with regional character. These structures and a lens of the Lagoa Meia Lua Formation appear to delimit the Passo do Ivo Formation. In depth, it is observed that the Passo do Ivo Formation has a continuity that exceeds 150 m in depth with a dip of 50 and azimuth of 220°.

The Palma Complex occurs over approximately 11.5 km along the profile, delineated by a magnetic high with a thickness of 4 km, which agrees with surface geology. The Palma Complex shows substantial indications of copper occurrences, as described in the literature by [4,16]. The MVI inversion shows subsurface continuity controlled by well-defined structural lineaments in previous geological mappings. The correlation of all this evidence of information indicates a high potential for copper occurrences associated with strong MVI anomalies. The magnetic anomaly is observed to be more intense at depth; it may be that this mineralized ultramafic body is increasing in depth and under strong structural control.

Following the profile, after the Palma Complex, the Pontas do Salso Formation occurs over approximately 17 km along the profile, represented by epiclastic metasedimentary rocks and metavolcanic tuffs. A low magnetic and low radioelement signature is observed, followed by a high magnetic marking (similar to another previous section) of the presence of magnesian schists of the Palma Complex.

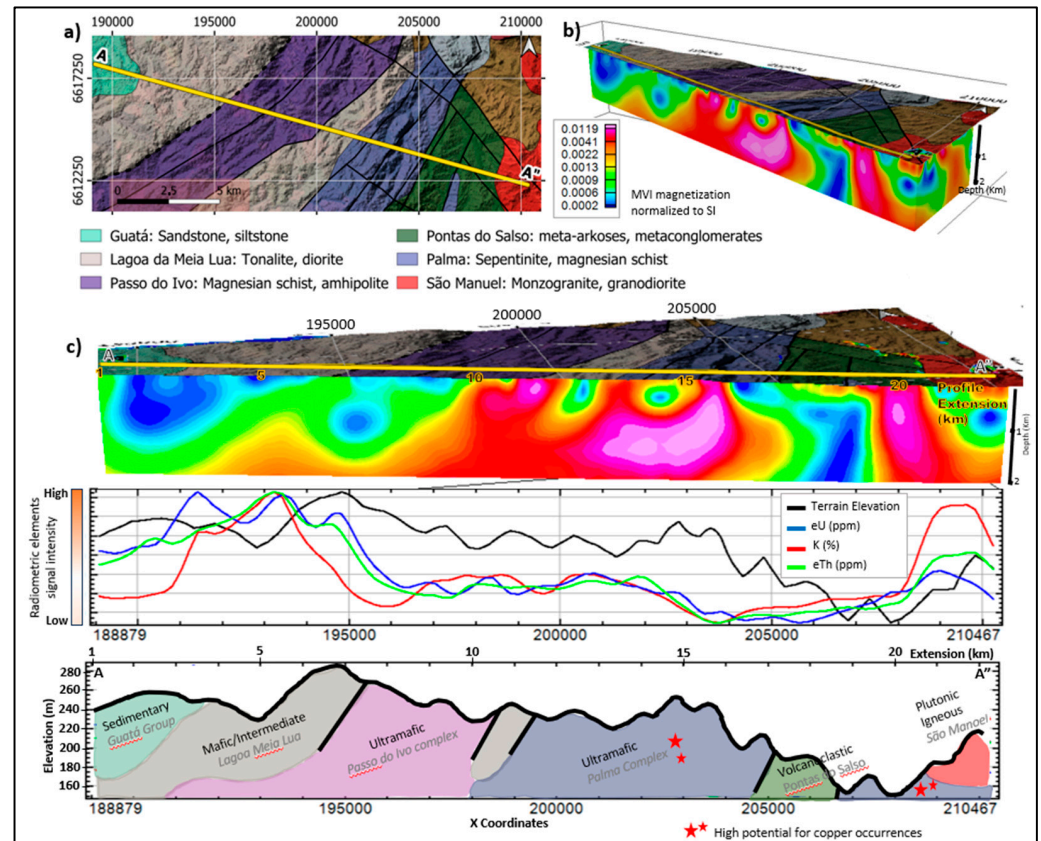


Figure 9. (a) Lithogeophysical Profile A–A'', (b) view of the MVI-generated inversion model. (c) A mosaic presenting the MVI-generated inversion model, graph with radioelement (K, eTh, eU) variations, and interpreted lithogeophysical profile.

At approximately 20.5 km along the profile, a significant increase in the signal intensity of the three radioelements combined with low magnetics near the surface is observed. Thus, it is interpreted that this response is related to the São Manuel Monzogranites and Granodiorites. However, it is suggested that the Palma Complex may also be present at greater depth due to strong magnetic anomalies. This region is also considered to have a high potential for copper occurrences. The contact between the ultramafic rock and plutonic igneous rocks may be favorable for sulfide presence. The lens of the Palma Complex has a greater extent than represented on the surface, extending to approximately 2 km in depth (Figure 9b).

The B–B'' profile aims to show the relationship between soil and stream sediment geochemical results with MVI data inversion, which may be related to the continuity of host bodies and/or directly related to mineralization (Figure 10). It can be observed that in the section parallel to the mineralized structures with azimuth 225°, parallel to the fracture related to the mineralizations, the body shows continuity in depth. The profile cut with a northward direction shows a tendency for continuity towards N45° E.

The MVI inversion model presents more than one magnetic body, and several mineral occurrences have been identified at the surface. Therefore, the study area may have several mineralized bodies that continue in extension and laterally. The structural control of the preferential direction N45° E somehow controls all. Most of those showing more excellent continuity are located near the contact zone between the Jaguarari Granite, the Palma Complex, and the Pontas do Salso Formation.

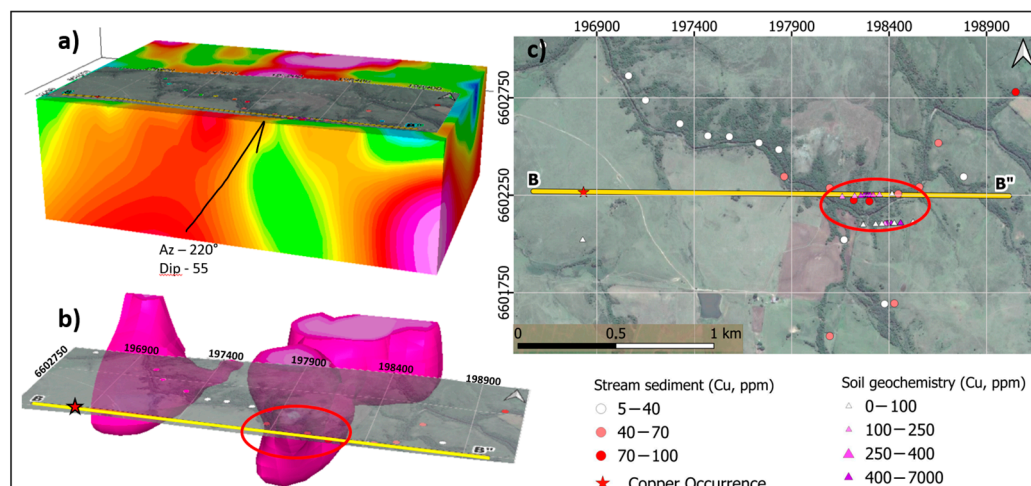


Figure 10. (a) MVI Model of Profile B–B'', (b) separation of selected MVI higher anomalies, and (c) map of Profile B–B'' location.

6. Concluding Remarks

Based on the proposal of this study, the results were satisfactory because, using the suggested workflow, it was possible to delimit potential areas with pre-existing geological mapping data, results from geochemical analyses, structural context, and products from the processing of airborne geophysical data from magnetometry and gamma spectrometry to understand the behavior of copper signatures in mafic-ultramafic bodies associated with copper occurrences in the Southern Rio Grande Shield. This geoscientific data processing and interpretation routine aims to advance and develop new research in the mineral exploration field in Brazil's southern portion and contribute to discoveries of metallic minerals with economic potential.

Processing aeromagnetic data using the first vertical derivative enhancement filter of the total anomalous magnetic field made it possible to relate the main structural lineaments. An MVI inversion model highlighted the continuities of the bodies in extension and depth.

The maps of the radioelements and ternary showed lithological contacts, and a table showing variations of the values generated from the interpolated airborne data was also presented. These can be used as parameters for future studies in the area and similar lithologies.

The profiles generated for litho-geophysical interpretation (Profile A–A with a length of 22 km) evidenced a detailed correlation of the radioelements delineating lithological contacts; the MVI inversion enriched the discussion on the continuity of ultramafic bodies such as the Palma Complex and on the structural framework delimiting regional structures in the preferred N45E direction. Cross-referencing historical data with new processing suggested areas with high potential for copper occurrences. Profile B–B'' achieved satisfactory results in verifying anomalies generated from the MVI inversion. These significantly correlate with historical results from sediment and soil geochemical analyses.

Author Contributions: Conceptualization, M.M.Z. and M.F.; methodology, M.M.Z.; software, M.M.Z.; validation, M.M.Z. and M.F.; formal analysis, M.F.; investigation, M.M.Z.; resources, M.M.Z.; data curation, M.M.Z. and M.F.; writing—original draft preparation, M.M.Z.; writing—review and editing, M.M.Z.; visualization, M.M.Z.; supervision, M.F.; project administration, M.F. All authors have read and agreed to the published version of the manuscript.

Funding: This research received no external funding.

Data Availability Statement: The data is available in the article. For detailed processing information, contact marielizago@gmail.com.

Conflicts of Interest: The authors declare no conflict of interest.

References

1. Attwood, J. Especialistas Alertam Para Possível Crise de Cobre que Frearia a Economia Global. Blog Bloomberg Linea Brasil. 2022. Available online: <https://www.bloomberglinea.com.br/2022/09/25/especialistas-alertam-para-possivel-crise-de-cobre-que-frearia-a-economia-global/> (accessed on 19 September 2023).
2. Oliveira, D.S. Uso da Geofísica No Atual Cenário da Exploração Mineral—Como Adicionar Valor Num Contexto Desafiador. *Boletim SBGf* **2024**, *130*, 18–21. Available online: https://sbgf.org.br/boletim/reader/boletim_130/ (accessed on 16 April 2024).
3. Costa, I.S.L. Desafios e Oportunidades da Geofísica na Descoberta de Recursos Minerais no Brasil. *Boletim SBGf* **2024**, *130*, 22–24. Available online: https://sbgf.org.br/boletim/reader/boletim_130/ (accessed on 16 April 2024).
4. Ribeiro, M.J. Mapa Previsional do Cobre no Escudo Sul—Rio-Grandense. In *Nota Explicativa*; Departamento Nacional da Produção, Ministério de Minas e Energia: Brasília, Brazil, 1978; 104p.
5. Wilford, J.; Bierwirth, P.; Craig, M. Application of gamma-ray spectrometry in soil/regolith mapping and geomorphology. *J. Geochem. Explor.* **1997**, *60*, 217–226.
6. Reeves, C. *Aeromagnetic Surveys: Principles, Practice and Interpretation*; Earth-Works: Washington, DC, USA, 2005; 155p.
7. Breustedt, B.; Höck, V.; Wiedenbeck, M. Geophysical and geochemical exploration for copper in the Central African Copperbelt. *Econ. Geol.* **2011**, *106*, 693–716.
8. Clark, D.A. Magnetic petrology and magnetic susceptibility of minerals. *Explor. Geophys.* **1997**, *28*, 62–71.
9. Hasui, Y.; Carneiro, C.D.R.; Coimbra, A.M. The Ribeira Folded Belt. *Rev. Bras. Geociências* **1975**, *5*, 257–266. [CrossRef]
10. Almeida, F.F.M.; Hasui, Y.; Brito Neves, B.B.; Fuck, R.A. Brazilian structural provinces: An introduction. *Earth Sci. Rev.* **1981**, *17*, 1–29. [CrossRef]
11. Hartmann, L.A.; Chemale, F.; Philipp, R.P. Evolução geotectônica do Rio Grande do Sul no Pré-Cambriano. In *50 Anos de Geologia: Instituto de Geociências*; Iannuzzi, R., Frantz, J.C., Eds.; Editora Comunicação e Identidade: Paulista, Brazil, 2007; pp. 97–123. Available online: http://multimidia.ufrgs.br/conteudo/bibgeo/repositorio/memorial/1998-2007/50anoscontribuicoes/50_anos_contribuicoes.pdf (accessed on 12 November 2023) ISBN 978859857303-8.
12. Hartmann, L.; Nardi, L.; Formoso, M.; Remus, M.; DE Lima, E.; Mexias, A. Magmatism and metallogeny in the crustal evolution of Rio Grande do Sul shield, Brazil. *Pesquisas* **1999**, *26*, 45–63. [CrossRef]
13. Hartmann, L.A.; Leite, J.A.D.; Da Silva, L.C.; Remus, M.V.D.; McNaughton, N.J.; Groves, D.I.; Fletcher, I.R.; Santos, J.O.S.; Vasconcellos, M.A.Z. Advances in SHRIMP geochronology and their impact on understanding the tectonic and metallogenic evolution of southern Brazil. *Aust. J. Earth Sci.* **2000**, *47*, 829–844. [CrossRef]
14. Babinski, M.; Chemale, F.; Hartmann, L.A.; Van Schmus, W.R.; da Silva, L.C. Juvenile accretion at 750–700 Ma in southern Brazil. *Geology* **1996**, *24*, 439–442. [CrossRef]
15. Hartmann, L.; Philipp, R.; Santos, J.; McNaughton, N. Time frame of 753–680 Ma juvenile accretion during the São Gabriel orogeny, southern Brazilian Shield. *Gondwana Res.* **2011**, *19*, 84–99. [CrossRef]
16. CPRM—Companhia de Pesquisa de Recursos Minerais. Mapa e Arquivos Vetoriais de Associações Tectônicas e Recursos Minerais Escudo Sul-Rio-Grandense. Escala 1:500.000. 2021. Available online: <https://geosgb.sgb.gov.br/downloads/> (accessed on 20 February 2024).
17. Almeida, I. Geologia da Jazida de Mármore de Palma, Município de São Gabriel, Rio Grande do Sul. In Congresso Brasileiro de Geologia. 1970, p. 138. Available online: https://www.sbgf.org.br/anais_digitalizados/1970-BRASILIA/CBG1970.pdf (accessed on 15 February 2024).
18. Vilwock, J.; Jost, H. Mineralizações de cobre, molibdênio e ouro nas cabeceiras do rio Vacacaí, São Gabriel. In *Congresso Brasileiro de Geologia*, 21; Anais: Curitiba, Brazil, 1967; pp. 80–102.
19. Ford, K.; Keating, P.; Thomas, M.D. *Overview of Geophysical Signatures Associated with Canadian ore Deposits*; Geological Association of Canada, Mineral Deposits Division, Special Publication: St. John's, NL, Canada, 2007; pp. 939–970. Available online: <https://ostrnrcan-dostrnrcan.canada.ca/handle/1845/181490> (accessed on 16 April 2024).
20. Sampaio, R.P.; Silva, J.C.; Ferreira, M.A. Aplicação de dados aerogamaespectrométricos para identificação de anomalias radiométricas em áreas de cobre e ferro no estado de Alagoas, Brasil. *Rev. Bras. Geofísica* **2024**, *42*, 23–35.
21. Ogah, J.A.; Abubakar, F. Solid mineral potential evaluation using integrated aeromagnetic and aeroradiometric datasets. *Nature. Sci. Rep.* **2024**, *14*, 1637. [CrossRef]
22. Dickson, B.L.; Scott, K.M. Interpretation of aerial gamma-ray surveys—Adding the geochemical factors. *AGSO J. Aust. Geol. Geophys.* **1997**, *17*, 187–200.
23. Souza, J.L.; Ferreira, F.J.F. Anomalias aerogamaespectrométricas (K, eU e eTh) da quadrícula de Araras (SP) e suas relações com processos pedogenéticos e fertilizantes fosfatados. *Rev. Bras. Geofísica* **2005**, *23*, 251–274. [CrossRef]

24. Silva, E.O.; Costa, S.S.; Feitoza, L.M. Caracterização Litogeofísica da Folha Rio Mucajaí, Estado de Roraima. Anais XIII Simpósio Brasileiro de Sensoriamento Remoto. 2007, pp. 6183–6190. Available online: <http://marte.sid.inpe.br/col/dpi.inpe.br/sbsr@80/2006/11.15.23.57.32/doc/6183-6190.pdf> (accessed on 15 April 2024).
25. Ferreira, F.J.F.; Fruchting, A.; Guimarães, G.B.; Alves, L.S.; Martin, V.M.O.; Ulbrich, H.H.G.J. Levantamentos Gamaespectrométricos em Granitos Diferenciados. II: O Exemplo do Granito Joaquim Murtinho, Complexo Granítico Cunhaporanga, Paraná. *Rev. Inst. Geociências—USP* **2009**, *9*, 55–72. [[CrossRef](#)]
26. Mero, J.L. Uses of the gamma-ray spectrometer in mineral exploration. *Geophysics* **1960**, *25*, 1054–1076. [[CrossRef](#)]
27. Shives, R.B.K.; Ford, K.L.; Peter, J.M. Mapping and Exploration Applications of Gamma Ray Spectrometry in the Bathurst Mining Camp, Northeastern New Brunswick. In *Massive Sulfide Deposits of the Bathurst Mining Camp, New Brunswick, and Northern Maine*; Society of Exploration Geophysicists: Tulsa, OK, USA, 2003. [[CrossRef](#)]
28. Hegab, M.A.E.R.; Salem, S.M. Mineral-bearing alteration zones at Gebel Monqul area, North Eastern Desert, Egypt, using remote sensing and gamma-ray spectrometry data. *Arab. J. Geosci.* **2021**, *14*, 1869. [[CrossRef](#)]
29. Alhumimidi, M.S.; Aboud, E.; Alqahtani, F.; Al-Battahien, A.; Saud, R.; Alqahtani, H.H.; Aljuhani, N.; Alyousif, M.M.; Alyousef, K.A. Gamma-ray spectrometric survey for mineral exploration at Baljurashi area, Saudi Arabia. *J. Radiat. Res. Appl. Sci.* **2021**, *14*, 82–90. [[CrossRef](#)]
30. Kearey, P.; Brooks, M.; Hill, I. *Geofísica de Exploração*; Oficina de textos: São Paulo, Brazil, 2009; 438p, ISBN 978-85-86238-91-8.
31. Kwan, K.; Müller, D. Mount Milligan alkalic porphyry Au–Cu deposit, British Columbia, Canada, and its AEM and AIP signatures: Implications for mineral exploration in covered terrains. *J. Appl. Geophys.* **2020**, *180*. [[CrossRef](#)]
32. Uwiduhaye, J.; Ngaruye, J.C.; Saibi, H. Defining potential mineral exploration targets from the interpretation of aeromagnetic data in Western Rwanda. *Ore Geol. Rev.* **2021**, *128*, 103927. [[CrossRef](#)]
33. Djomo, H.D.; Sezine, E.D.; Yandjmain, J. Integration of airborne magnetic and geological data for mineral prospectivity mapping in the Ambam-Amvom rainforest area, Archean Ntem Complex, southern Cameroon. *Sci. Afr.* **2024**, *24*, e02157. [[CrossRef](#)]
34. Kwan, K.; Reford, S. Innovative airborne geophysical strategies to assist the exploration of critical metal systems. *Geosystems and Geoenvironment.* **2025**, *4*. [[CrossRef](#)]
35. Willocks, A.J. Geophysical responses for copper mineralization associated with iron deposits at Nowa Nowa. *ASEG Ext. Abstr.* **1999**, *1999*, 149–162. [[CrossRef](#)]
36. CPRM—Companhia de Pesquisa de Recursos Minerais. Projeto Aerogeofísico Escudo do Rio Grande do Sul—Dados em XYZ e Relatório Final do Levantamento e Processamento dos Dados Magnetométricos e Gamaespectrométricos. 2010. Available online: <https://geosgb.sgb.gov.br/downloads/> (accessed on 24 February 2024).
37. Nabighian, M.N. The analytic signal of two-dimensional magnetic bodies with polygonal cross-section. Its properties and use for automated anomaly interpretation. *Geophysics* **1972**, *37*, 507–517. [[CrossRef](#)]
38. MacLeod, I.C.; Jones, K.; Dai, T.F. 3-D analytic signal in the interpretation of total magnetic field data at low magnetic latitudes. *Explor. Geophys.* **1993**, *24*, 679–688. [[CrossRef](#)]
39. Debeglia, N.; Corpel, J. Automatic 3-D interpretation of potential field data using analytic signal derivatives. *Geophysics* **1997**, *6*, 87–96. [[CrossRef](#)]
40. Blakely, R.J. *Potential Theory in Gravity and Magnetic Applications*; Cambridge University Press: Cambridge, UK, 1995.
41. Reynolds, J.M. *An Introduction to Applied and Environmental Geophysics*, 2nd ed.; Wiley: Chichester, UK, 2011.
42. Peters, L.J. The direct approach to magnetic interpretation and its practical application. *Geophysics* **1949**, *14*, 290–320. [[CrossRef](#)]
43. Nettleton, L.L. Regionals, residuals, and structures. *Geophysics* **1954**, *19*, 1–22. [[CrossRef](#)]
44. Dean, W.C. Frequency analysis for gravity and magnetic interpretation. *Geophysics* **1958**, *23*, 97–127. [[CrossRef](#)]
45. Clement, W.G. Basic principles of two-dimensional digital filtering. *Geophysics* **1973**, *21*, 125–145. [[CrossRef](#)]
46. Hinze, W.J.; Von Frese, R.R.B.; Saad, A.H. *Gravity and Magnetic Exploration: Principles, Practices, and Applications*; Cambridge University Press: New York, NY, USA, 2013; 512p, ISBN 978-0-521-87101-3.
47. Nabighian, M.N. Additional comments on the analytic signal of two-dimensional magnetic bodies with polygonal cross-section. *Geophysics* **1974**, *39*, 85–92. [[CrossRef](#)]
48. Nabighian, M.N. Toward a three-dimensional automatic interpretation of potential field data via generalized Hilbert transforms Fundamental relations. *Geophysics* **1984**, *49*, 780–786. [[CrossRef](#)]
49. Atchuta Rao, D.; Ram Babu, H.V.; Sanker Narayan, P.V. Interpretation of magnetic anomalies due to dikes: The complex gradient method. *Geophysics* **1981**, *46*, 1572–1578. [[CrossRef](#)]
50. Oldenburg, D.W.; Pratt, D.A. Geophysical Inversion for Mineral Exploration: A Decade of Progress in Theory and Practice. In *Proceedings of the Exploration 07: Fifth Decennial International Conference on Mineral Exploration*, Toronto, ON, Canada, 9–12 September 2007; pp. 61–95.
51. Shearer, S.; Li, Y. 3D Inversion of magnetic total gradient data in the presence of remanent magnetization. In *SEG Technical Program Expanded Abstracts*; Society of Exploration Geophysicists: Tulsa, OK, USA, 2004; pp. 774–777. [[CrossRef](#)]

52. Li, Y.; Shearer, S.E.; Haney, M.M.; Dannemiller, N. Comprehensive approaches to 3D inversion of magnetic data affected by remanent magnetization. *Geophysics* **2010**, *75*, L1–L11. [[CrossRef](#)]
53. Ellis, R.G.; Wet, B.; McLeod, I.N. Inversion of Magnetic Data from Remanent and Induced Sources. *ASEG Ext. Abstr.* **2012**, *2012*, 1–4. [[CrossRef](#)]
54. Bocci, P.; Ribeiro, M.J. Mapeamento Preliminar Geológico da Área n.5 da Quadricula Arroio São Sepé. Master's Thesis, Federal University of Rio Grande do Sul (UFRGS), Porto Alegre, Brazil, 1963.

Disclaimer/Publisher's Note: The statements, opinions and data contained in all publications are solely those of the individual author(s) and contributor(s) and not of MDPI and/or the editor(s). MDPI and/or the editor(s) disclaim responsibility for any injury to people or property resulting from any ideas, methods, instructions or products referred to in the content.